Inorg. Chem. **2008**, *47*, 4832−4843

Inorganic Chemistry
Article

Single-Molecule Magnets: A Family of Mn^{III}/Ce^{IV} Complexes with a $[Mn_8CeO_8]^{12+}$ Core

Abhudaya Mishra,[†] Anastasios J. Tasiopoulos,[†,‡] Wolfgang Wernsdorfer,[§] Eleni E. Moushi,[‡] Brian Moulton,[||] Michael J. Zaworotko,[||] Khalil A. Abboud,[†] and George Christou*,[†]

Department of Chemistry, University of Florida, Gainesville, Florida 32611-7200, Department of Chemistry, University of Cyprus, 1678 Nicosia, Cyprus, Institut Néel, CNRS/UJF, BP 166, 25 Avenue des Martyrs, 38042 Grenoble, Cedex 9, France, and Department of Chemistry, University of South Florida, Tampa, Florida 33620

Received January 21, 2008

Four heterometallic, enneanuclear Mn_8Ce clusters $[Mn_8CeO_8(O_2CMe)_{12}(H_2O)_4]$ (**4**), $[Mn_8CeO_8(O_2CMe)_{12}(py)_4]$ (**5**), $[Mn_8CeO_8(O_2CPh)_{12}(MeCN)_4]$ $[Mn_8CeO_8(O_2CPh)_{12}(dioxane)_4]$ (**6**), and $[Mn_8CeO_8(O_2CCHPh_2)_{12}(H_2O)_4]$ (**7**) have been prepared by various methods. Their cores are essentially isostructural and comprise a nonplanar, saddlelike $[Mn^{III}_8O_8]^{8+}$ loop containing a central Ce^{IV} ion attached to the eight μ_3-O^{2-} ions. Peripheral ligation around the $[Mn_8CeO_8]^{12+}$ core is provided by eight μ- and four μ_3-O_2CR^- groups. Terminal ligation on four Mn^{III} atoms is provided by H_2O in **4** and **7**, pyridine in **5**, and MeCN/dioxane in **6**. Solid-state magnetic susceptibility studies, fits of dc magnetization vs field and temperature data, and in-phase ac susceptibility studies in a zero dc field have established that complexes **4**, **5**, and **7** possess $S = 16$, $S = 4$ or 5, and $S = 6 \pm 1$ spin ground states, respectively, but in all cases there are very low-lying excited states. The large variation in the ground-state spins for this isostructural family is rationalized as due to a combination of weak exchange interactions between the constituent Mn^{III} atoms, and the presence of both nearest-neighbor and next-nearest-interactions of comparable magnitudes. Magnetization vs applied dc field sweeps on single crystals of $\mathbf{4}\cdot 4H_2O$ and $\mathbf{7}\cdot 4H_2O\cdot 3MeCN\cdot 2CH_2Cl_2$ down to 0.04 K have established that these two complexes are new single-molecule magnets (SMMs). The former also shows an exchange-bias, a perturbation of its single-molecule properties from very weak intermolecular interactions mediated by hydrogen-bonding interactions with lattice–water molecules of crystallization.

Introduction

One of the motivating themes in our polynuclear cluster chemistry is the identification of new high nuclearity manganese carboxylate clusters that can function as nanoscale magnetic materials. Because such species are molecular in nature, fall in the nanoscale size regime, and display superparamagnetlike slow magnetization relaxation as a result of intrinsic properties of individual molecules, they have been called single-molecule magnets (SMMs) or molecular nanomagnets. SMMs thus represent a molecular or "bottom-up" approach to nanomagnetism.[1] They exhibit hysteresis in magnetization versus dc field scans below their blocking temperature (T_B), with the relaxation barrier arising from the combination of a large ground-state spin (S) and a large and negative Ising- (easy-axis-) type of magnetoanisotropy, as measured by the axial zero-field splitting parameter, D. This leads to a significant barrier (U) to magnetization reversal, its maximum value given by $S^2|D|$ or $(S^2 - ¼)|D|$ for integer and half-integer spin, respectively.[1,2] However, in practice, quantum tunneling of the magnetization (QTM) through the barrier via higher lying M_S levels of the spin S manifold results in the actual or effective barrier (U_{eff}) being less than U. Indeed, a primary reason that SMMs have been of interest to scientists of various disciplines is this combination of their

* To whom correspondence should be addressed. Tel.: (352) 392-8314. Fax: (352) 392-8757. E-mail: christou@chem.ufl.edu.
[†] University of Florida.
[‡] University of Cyprus.
[§] Institut Néel.
[||] University of South Florida.

(1) (a) Christou, G.; Gatteschi, D.; Hendrickson, D. N.; Sessoli, R. *MRS Bull.* **2000**, *25*, 66. and references cited therein. (b) Aromi, G.; Aubin, S. M. J.; Bolcar, M. A.; Christou, G.; Eppley, H. J.; Folting, K.; Hendrickson, D. N.; Huffman, J. C.; Squire, R. C.; Tsai, H.-L.; Wang, S.; Wemple, M. W. *Polyhedron* **1998**, *17*, 3005. (c) Christou, G. *Polyhedron* **2005**, *24*, 2065.

10.1021/ic8001064 CCC: $40.75
Published on Web 04/15/2008

often aesthetically pleasing structures and their ability to display classical magnetic bistability and quantum properties, while at the same time retaining all the advantages of molecular species, such as crystallinity, solubility, and easy chemical modification in targeted ways.[2] The first SMM discovered was $[Mn_{12}O_{12}(O_2CMe)_{16}(H_2O)_4]$[2] (hereafter referred to as Mn_{12}-acetate), a member of the $[Mn_{12}O_{12}(O_2CR)_{16}(H_2O)_4]$ (Mn_{12}; R = various) family of molecules with an $S = 10$ ground state; these complexes are still the most thoroughly studied SMMs to date.[2,3] There are also now many other structural types of SMMs known, spanning several metals, but most of them are completely or primarily Mn^{III} complexes.[4–7]

As part of a continuing development of new synthetic routes to novel structural types that can function as SMMs, we and several other groups have been exploring 3d/4d, 3d/5d, and 3d/4f mixed-metal cluster complexes that have the appropriate properties to function as SMMs.[8] Our own contributions to this relatively new field have included Mn_8Ce,[9] $Mn_{11}Dy_4$,[10a] Mn_2Dy_2,[10b] and Fe_2Dy_2[10c] SMMs. Our original communication of the Mn_8Ce SMM, which possesses an $S = 16$ ground state, described how it was obtained by a template synthesis using a Ce^{IV} ion around which formed a ferromagnetically coupled loop of Mn^{III} ions. We have since extended and expanded this work and in this paper report full details of the syntheses, structures, magnetic characterization, and reactivity of four structurally related Mn_8Ce complexes. We shall show that some are new SMMs and that they also demonstrate extensive spin-variability within the family.

Experimental Section

Syntheses. All manipulations were performed under aerobic conditions using chemicals as received, unless otherwise stated. $\{[Mn(OH)(O_2CMe)_2]\cdot(MeCO_2H)\cdot(H_2O)\}_n$ (**1**),[11] $[Mn_3O(O_2CMe)_6(py)_3]$ (**2**),[12a] and $(NBu^n_4)[Mn_4O_2(O_2CPh)_9(H_2O)]$ (**3**),[12b] were prepared as previously described.

$[Mn_8CeO_8(O_2CMe)_{12}(H_2O)_4]$ (4). Method A. To a slurry of **1** (2.00 g, 7.46 mmol) in MeCN (35 mL) was added solid $(NH_4)_2Ce(NO_3)_6$ (0.51 g, 0.93 mmol), and the mixture was left under magnetic stirring for 8 h. This gave some brown powder and a reddish-brown solution, which were separated by filtration. To the filtrate was added Et_2O (40 mL), and the solution left under magnetic stirring for 5 min and refiltered. This filtrate was

(2) (a) Sessoli, R.; Gatteschi, D.; Caneschi, A.; Novak, M. A. *Nature* **1993**, *365*, 141. (b) Sessoli, R.; Ysai, H.-L.; Schake, A. R.; Wang, S.; Vincent, J. B.; Folting, K.; Gatteschi, D.; Christou, G.; Hendrickson, D. N. *J. Am. Chem. Soc.* **1993**, *115*, 1804. (c) Thomas, L.; Lionti, L.; Ballou, R.; Gatteschi, D.; Sessoli, R.; Barbara, B. *Nature* **1996**, *383*, 145.

(3) (a) Eppley, H. J.; Tsai, H.-L.; de Vries, N.; Folting, K.; Christou, G.; Hendrickson, D. N. *J. Am. Chem. Soc.* **1995**, *117*, 301. (b) Aubin, S. M. J.; Spagna, S.; Eppley, H. J.; Sager, R. E.; Christou, G.; Hendrickson, D. N. *Chem. Commun.* **1998**, 803. (c) Aubin, S. M. J.; Sun, Z.; Pardi, L.; Krzystek, J.; Folting, K.; Brunel, L.-C.; Rheingold, A. L.; Christou, G.; Hendrickson, D. N. *Inorg. Chem.* **1999**, *38*, 5329. (d) Soler, M.; Chandra, S. K.; Ruiz, D.; Davidson, E. R.; Hendrickson, D. N.; Christou, G. *Chem. Commun.* **2000**, 2417. (e) Boskovic, C.; Pink, M.; Huffman, J. C.; Hendrickson, D. N.; Christou, G. *J. Am. Chem. Soc.* **2001**, *123*, 9914. (f) Artus, P.; Boskovic, C.; Yoo, J.; Streib, W. E.; Brunel, L.-C.; Hendrickson, D. N.; Christou, G. *Inorg. Chem.* **2001**, *40*, 4199. (g) Soler, M.; Wernsdorfer, W.; Abboud, K. A.; Huffman, J. C.; Davidson, E. R.; Hendrickson, D. N.; Christou, G. *J. Am. Chem. Soc.* **2003**, *125*, 3576. (h) Chakov, N. E.; Wernsdorfer, W.; Abboud, K. A.; Hendrickson, D. N.; Christou, G. *Dalton Trans.* **2003**, 2243. (i) Morello, A.; Bakharev, O. N.; Brom, H. B.; de Jongh, L. J. *Polyhedron* **2003**, *22*, 1745. (j) Bian, G. -Q.; Kuroda-Sowa, T.; Konaka, H.; Hatano, M.; Maekawa, M.; Munakata, M.; Miyasaka, H.; Yamashita, M. *Inorg. Chem.* **2004**, *43*, 4790. (k) Ruiz, D.; Sun, Z.; Albela, B.; Folting, K.; Ribas, J.; Christou, G.; Hendrickson, D. N. *Angew. Chem., Int. Ed.* **1998**, *37*, 300. (l) Aubin, S. M. J.; Sun, Z.; Guzei, I. A.; Rheingold, A. L.; Christou, G.; Hendrickson, D. N. *J. Chem. Soc., Chem. Commun.* **1997**, 2239.

(4) (a) Miyasaka, H.; Clérac, R.; Wernsdorfer, W.; Lecren, L.; Bonhomme, C.; Sugiura, K.; Yamashita, M. A. *Angew. Chem., Int. Ed.* **2004**, *43*, 2801. (b) Milios, C. J.; Raptopoulou, C. P.; Terzis, A.; Lloret, F.; Vicente, R.; Perlepes, S. P.; Escuer, A. *Angew. Chem., Int. Ed.* **2003**, *43*, 210. (c) Brechin, E. K.; Soler, M.; Davidson, J.; Hendrickson, D. N.; Parsons, S.; Christou, G. *Chem. Commun.* **2002**, 2252. (d) Price, D. J.; Batten, S. R.; Moubaraki, B.; Murray, K. S. *Chem. Commun.* **2002**, 762. (e) Brechin, E. K.; Boskovic, C.; Wernsdorfer, W.; Yoo, J.; Yamaguchi, A.; Sanado, E. C.; Concolino, T. R.; Rheingold, A. L.; Ishimoto, H.; Hendrickson, D. N.; Christou, G. C. *J. Am. Chem. Soc.* **2002**, *124*, 9710. (f) Sanudo, E. C.; Wernsdorfer, W.; Abboud, K. A.; Christou, G. *Inorg. Chem.* **2004**, *43*, 4137. (g) Tasiopoulos, A. J.; Vinslava, A.; Wernsdorfer, W.; Abboud, K. A.; Christou, G. *Angew. Chem., Int. Ed.* **2004**, *43*, 2117. (h) Tasiopoulos, A. J.; Wernsdorfer, W.; Abboud, K. A.; Christou, G. *Angew. Chem., Int. Ed.* **2004**, *43*, 6338. (i) Zaleski, C. M.; Depperman, E. C.; Dendrinou-Samara, C.; Alexiou, M.; Kampf, J. W.; Kessissoglou, D. P.; Kirk, M. L.; Pecoraro, V. L. *J. Am. Chem. Soc.* **2005**, *127*, 12862.

(5) (a) Brechin, E. K.; Yoo, J.; Huffman, J. C.; Hendrickson, D. N.; Christou, G. *Chem Commun.* **1999**, 783. (b) Yoo, J.; Brechin, E. K.; Yamaguchi, A.; Nakano, M.; Huffman, J. C.; Maniero, A. L.; Brunel, L.-C.; Awaga, K.; Ishimoto, H.; Christou, G.; Hendrickson, D. N. *Inorg. Chem.,* **2000**, *39*, 3615. (c) Yoo, J.; Yamaguchi, A.; Nakano, M.; Krzystek, J.; Streib, W. E.; Brunel, L.-C.; Ishimoto, H.; Christou, G.; Hendrickson, D. N. *Inorg. Chem.* **2001**, *40*, 4604. (d) Lecren, L.; Wernsdorfer, W.; Li, Y.-G.; Roubeau, O.; Miyasaka, H.; Clerac, R. *J. Am. Chem. Soc.* **2005**, *127*, 11311. (e) Lecren, L.; Roubeau, O.; Coulon, C.; Li, Y.-G.; Le Goff, X. F.; Wernsdorfer, W.; Miyasaka, H.; Clerac, R. *J. Am. Chem. Soc.* **2005**, *127*, 17353.

(6) (a) Aubin, S. M. J.; Wemple, M. W.; Adams, D. M.; Tsai, H.-L.; Christou, G.; Hendrickson, D. N. *J. Am. Chem. Soc.* **1996**, *118*, 7746. (b) Aubin, S. M.; Gilley, N. R.; Pardi, L.; Krzystek, J.; Wemple, M. W.; Brunel, L. C.; Marple, M. B.; Christou, G.; Hendrickson, D. N. *J. Am. Chem. Soc.* **1998**, *120*, 4991. (c) Andres, H.; Basler, R.; Gudel, H.-U.; Aromi, G.; Christou, G.; Buttner, H.; Ruffle, B. *J. Am. Chem. Soc.* **2000**, *122*, 12469–12477.

(7) (a) Foguet-Albiol, D.; O'Brien, T. A.; Wernsdorfer, W.; Moulton, B.; Zaworotko, M. J.; Abboud, K. A.; Christou, G. *Angew. Chem. Int. Ed.* **2005**, *44*, 897. (b) Rumberger, E. M.; Shah, S. J.; Beedle, C. C.; Zakharov, L. N.; Rheingold, A. L.; Hendrickson, D. N. *Inorg. Chem.* **2005**, *44*, 2742.

(8) (a) Sokol, J. J.; Hee, A. G.; Long, J. R. *J. Am. Chem. Soc.* **2002**, *124*, 7656. (b) Schelter, E. J.; Prosvirin, A. V.; Dunbar, K. R. *J. Am. Chem. Soc.* **2004**, *126*, 15004. (c) Osa, S.; Kido, T.; Matsumoto, N.; Re, N.; Pochaba, A.; Mrozinski, J. *J. Am. Chem. Soc.* **2004**, *126*, 420. (d) Zaleski, C. M.; Depperman, E. C.; Kampf, J. W.; Kirk, M. L.; Pecoraro, V. L. *Angew. Chem., Int. Ed.* **2004**, *43*, 3912. (e) Oshio, H.; Nihei, M.; Koizumi, S.; Shiga, T.; Nojiri, H.; Nakano, M.; Shirakawa, N.; Akatsu, M. *J. Am. Chem. Soc.* **2005**, *127*, 4568. (f) Costes, J.-P.; Dahan, F.; Wernsdorfer, W. *Inorg. Chem.* **2006**, *45*, 5. (g) Mori, F.; Nyui, T.; Ishida, T.; Nogami, T.; Choi, K.; Nojiri, H. *J. Am. Chem. Soc.* **2006**, *128*, 1440. (h) Zaleski, C. M.; Kampf, J. W.; Mallah, T.; Kirk, M. L.; Pecoraro, V. L. *Inorg. Chem.* **2007**, *46*, 1954. (i) Zaleski, C. M.; Depperman, E. C.; Kampf, J. W.; Kirk, M. L.; Pecoraro, V. L. *Inorg. Chem.* **2006**, *45*, 10022. (j) Aronica, C.; Pilet, G.; Chastanet, G.; Wernsdorfer, W.; Jacquot, J. -F.; Luneau, D. *Angew. Chem., Int. Ed.* **2006**, *45*, 4659.

(9) Tasiopoulos, A. J.; Wernsdorfer, W.; Moulton, B.; Zaworotko, M. J.; Christou, G. *J. Am. Chem. Soc.* **2003**, *125*, 15274.

(10) (a) Mishra, A.; Wernsdorfer, W.; Abboud, K. A.; Christou, G. *J. Am. Chem. Soc.* **2004**, *126*, 15648. (b) Mishra, A.; Wernsdorfer, W.; Parsons, S.; Christou, G.; Brechin, E. K. *Chem. Commun.* **2005**, 2086. (c) Murugesu, M.; Mishra, A.; Wernsdorfer, W.; Abboud, K. A.; Christou, G. *Polyhedron* **2006**, *25*, 613.

(11) Tasiopoulos, A. J.; Harden, N. C.; Abboud, K. A.; Christou, G. *Polyhedron* **2003**, *22*, 133.

(12) (a) Vincent, J. B.; Chang, H. R.; Folting, K.; Huffman, J. C.; Christou, G.; Hendrickson, D. N. *J. Am. Chem. Soc.* **1987**, *109*, 5703. (b) Wemple, M. W.; Tsai, H.-L.; Wang, S.; Claude, J.-P.; Streib, W. E.; Huffman, J. C.; Hendrickson, D. N.; Christou, G. *Inorg. Chem.* **1996**, *35*, 6450.

Table 1. Crystallographic Data for Complexes **4**−**6**

	4·4H$_2$O	**4**·4H$_2$O·4MeCN	**5**·3C$_4$H$_8$O$_2$	**6**·12C$_4$H$_8$O$_2$·4MeOH
formula	$C_{24}H_{52}O_{40}Mn_8Ce$	$C_{32}H_{64}N_4O_{40}Mn_8Ce$	$C_{56}H_{80}N_4O_{38}Mn_8Ce$	$C_{236}H_{276}N_4O_{100}Mn_{16}Ce_2$
fw (g/mol)	1560.30	1724.49	1996.87	5927.99
space group	$I\bar{4}$	$I\bar{4}$	$P4_2/n$	$P4n2$
a Å	23.947(6)	24.6153(6)	12.7367(6)	22.5647(6)
b Å	23.947(6)	24.6153(6)	12.7367(6)	22.5647(6)
c Å	9.953(5)	10.1274(2)	23.485(2)	26.3631(13)
β (deg)	90	90	90	90
V Å^3	5708(4)	6136.3(3)	3809.8(4)	13423.2(8)
Z	4	4	2	2
T K	100(2)	100(2)	173(2)	173(2)
radiation (Å)[a]	0.71073	0.71073	0.71073	0.71073
ρ_{calcd} (g/cm^3)	1.816	2.096	1.697	1.784
μ (mm^{-1})	2.584	3.143	1.953	1.168
R1[b,c]	0.0899	0.0285	0.0497	0.0367
wR2[d]	0.2115	0.0595	0.1165	0.1083

[a] Graphite monochromator. [b] $I > 2\sigma(I)$. [c] $R1 = 100[\Sigma(||F_o| - |F_c||)/\Sigma|F_o|$. [d] $wR2 = 100[\Sigma[w(F_o^2 - F_c^2)^2]/\Sigma[w(F_o^2)^2]]^{1/2}$, $w = 1/[\sigma^2(F_o^2) + [(ap)^2 + bp]$, where $p = [\max(F_o^2, O) + 2F_c^2]/3$.

concentrated slowly by evaporation over a few days to yield red-brown crystals of **4**·4H$_2$O·4MeCN, which were collected by filtration, washed with Me$_2$CO and Et$_2$O, and dried in vacuo; the yield was 55%. Anal. Calcd (Found) for **4**·4H$_2$O: $C_{24}H_{52}O_{40}Mn_8Ce$: C, 18.47 (18.49); H, 3.36 (3.32). Selected IR data (KBr, cm^{-1}): 3392(s, br), 1576(s), 1539(s), 1444(s), 1029(w), 680(s), 657(m), 619(m), 589(s, br), 551(m), 496(w), 432(w).

Method B. $[Mn_6CeO_9(O_2CMe)_9(NO_3)(H_2O)_2]$[13] (0.50 g, 0.38 mmol) was dissolved in MeCN (20 mL) and the mixture left under magnetic stirring for 20 min, filtered, and the filtrate layered with Et$_2$O (40 mL). After 2 weeks, the solution was filtered to remove some solid, and the filtrate slowly concentrated by evaporation to give red-brown crystals of **4**·4H$_2$O. These were filtered, washed with Me$_2$CO and Et$_2$O, and dried in vacuo; the yield was 5%. Anal. Calcd (Found) for **4**·4H$_2$O: $C_{24}H_{52}O_{40}Mn_8Ce$: C, 18.47 (18.40); H, 3.36 (3.30).

$[Mn_8CeO_8(O_2CMe)_{12}(py)_4]$ (5). To a slurry of **2** (1.00 g, 1.29 mmol) in MeCN (50 mL) was added solid $(NH_4)_2Ce(NO_3)_6$ (0.24 g, 0.43 mmol) and the mixture was left under magnetic stirring for 30 min. The solution was filtered and the filtrate layered with 1,4-dioxane (50 mL). After a week, well-formed square crystals of **5**·3C$_4$H$_8$O$_2$ were collected by filtration, washed with 1,4-dioxane and dried in vacuo; the yield was 60%. Anal. Calcd (Found) for **5**·3C$_4$H$_8$O$_2$: $C_{56}H_{80}N_4O_{38}Mn_8Ce$: C, 33.68 (33.75); H, 4.04 (4.15); N, 2.81 (2.54). Selected IR data (KBr, cm^{-1}): 3429(s, br), 1576(s), 1540(s), 1444(s), 1119(w), 871(w), 679(m), 656(m), 619(m), 589(s, br), 551(m), 496(w), 430(m).

$[Mn_8CeO_8(O_2CPh)_{12}(MeCN)_4][Mn_8CeO_8(O_2CPh)_{12}(dioxane)_4]$ (6). To a slurry of **3** (1.00 g, 0.62mmol) in MeCN/MeOH (25/1 mL) was added solid $(NH_4)_2Ce(NO_3)_6$ (0.34 g, 0.62mmol) and the mixture was left under magnetic stirring for 20 min. The solution was filtered and the filtrate layered with 1,4-dioxane (25 mL). After a week, large dark red crystals of **6**·12C$_4$H$_8$O$_2$·4MeOH were collected by filtration, washed with 1,4-dioxane, and dried briefly in vacuo; the yield was 45% based on Ce. Anal. Calcd (Found) for **6**·12C$_4$H$_8$O$_2$·4MeOH: $C_{236}H_{276}N_4O_{100}Mn_{16}Ce_2$: C, 47.82 (48.00); H, 4.69 (4.60); N 0.95 (0.90). Selected IR data (KBr, cm^{-1}): 3430(s, br), 1600(m), 1560(s), 1528(s), 1412(s), 1120(w), 872(w), 718(s), 683(m), 615(m), 573(s, br), 510(w), 422(w).

$[Mn_8CeO_8(O_2CCHPh_2)_{12}(H_2O)_4]$ (7). To a slurry of complex **4** (0.20 g, 0.12mmol) in MeCN (50 mL) was added diphenylacetic acid (0.54 g, 2.5 mmol) and the mixture stirred overnight. To the resulting solution was added toluene (50 mL), and the solvent removed by rotoevaporation to remove acetic acid as its toluene azeotrope. Three cycles of dissolution of the residue in MeCN, addition of toluene, and removal of solvent by rotoevaporation were carried out. The resulting solid was then redissolved in MeCN (20 mL), and the solution left to concentrate by slow evaporation to give large, well-formed black crystals. These were recrystallized from a CH_2Cl_2/heptanes layering, which gave black crystals of **7**·4H$_2$O·3MeCN·2CH$_2$Cl$_2$ after 1 week. The crystals were collected by filtration, washed with heptanes and dried in vacuo; the overall yield was 60%. The synthesis can also be performed using complex **5** instead of **4** as the starting material. Vacuum-dried solid analyzed as **7**·4H$_2$O. Anal. Calcd (Found) for $C_{168}H_{148}O_{40}Mn_8Ce$: C, 59.58 (59.45); H, 4.40 (4.25). Selected IR data (KBr, cm^{-1}): 3429(s, br), 1590(m), 1550(s), 1527(m), 1494(w), 1404(s), 1032(w), 745(m), 697(s), 650(m), 580(s, br), 433(w).

X-ray Crystallography. For **4**·4H$_2$O, **5**·3C$_4$H$_8$O$_2$, **6**·12C$_4$H$_8$O$_2$·4MeOH and **7**·4H$_2$O·3MeCN·2CH$_2$Cl$_2$, data were collected on a Siemens SMART PLATFORM whereas for **4**·4H$_2$O·4MeCN data were collected on an Oxford-Diffraction Xcalibur diffractometer, both equipped with a CCD area detector and a graphite monochromator utilizing Mo Kα radiation ($\lambda = 0.71073$ Å). Suitable crystals were attached to glass fibers using silicone grease and transferred to a goniostat where they were cooled for data collection. Cell parameters were refined using up to 12766 reflections. The first 50 frames were remeasured at the end of data collection to monitor instrument and crystal stability (maximum correction on I was <1%). Absorption corrections by integration were applied based on measured indexed crystal faces. The structures were solved by direct methods,[14] and refined on F^2 using full-matrix least-squares.[14] The non-H atoms were treated anisotropically, whereas the hydrogen atoms were placed in calculated, ideal positions and refined as riding on their respective carbon atoms. Unit-cell data and structure refinement details are listed in Table 1.

For **4**·4H$_2$O and **4**·4H$_2$O·4MeCN, there are two symmetry-independent molecules in the unit cell, both lying on S_4 symmetry axes parallel to the crystal c axis. The two molecules are essentially superimposable. The water molecules of crystallization each hydrogen-bond to two adjacent Mn_8Ce clusters and form one-dimensional, hydrogen-bonded chains of Mn_8Ce clusters parallel to the crystal c axis. Thus, O1W hydrogen-bonds to bound water O6 (O1W···O6 = 2.645 for **4**·4H$_2$O and 2.750 Å for **4**·4H$_2$O·4MeCN), μ_3-O^{2-} ion O1 (O1W···O1 = 2.616 and 2.756

(13) (a) Tasiopoulos, A. J.; O'Brien, T. A.; Abboud, K. A.; Christou, G. 2008, unpublished results. (b) Tasiopoulos, A. J.; O'Brien, T. A.; Abboud, K. A.; Christou, G. *Angew. Chem., Int. Ed.* **2004**, *43*, 345.

(14) (a) Sheldrick, G. M. *Acta Crystallogr., Sect. A* **1990**, *46*, 467;. SHELX86. (b) Sheldrick, G. M. *SHELXL-97*; University of Göttingen: Göttingen, Germany, 1997. (c) Spek, A. L. *Acta Crystallogr., Sect. A* **1990**, *46*, C34.

Å) and acetate O atom O2 (O1W···O2 = 2.842 and 3.036 Å) on one Mn_8Ce cluster, and bound water O6 (O1W···O6 = 2.743 and 2.716 Å) on the neighboring Mn_8Ce cluster. These intermolecular hydrogen-bonding interactions are of importance to the magnetic properties to be described later (vide infra). A total of 342 parameters for **4**·$4H_2O$ and 399 for **4**·$4H_2O$·4MeCN were included in the refinement using 2958 and 7040 reflections, respectively, with $I > 2\sigma(I)$. We report the crystal structures of both forms of **4** because the magnetic studies were performed on **4**·$4H_2O$, whereas the structure of **4**·$4H_2O$·4MeCN was obtained more recently to provide more reliable metric parameters. The low quality crystal analysis of **4**·$4H_2O$ is primarily due to the small size of the crystals, which however did not affect the magnetism studies. For **5**·$3C_4H_8O_2$, there is only one type of molecule by symmetry in the unit cell, lying on an S_4 axis parallel to the crystal *c* axis. There are also three dioxane molecules, lying on a 2-fold rotation axis or a S_4 axis. A total of 258 parameters were included in the refinement using 23703 reflections with $I > 2\sigma(I)$. For **6**·$12C_4H_8O_2$·4MeOH, there are two types of molecules, both lying on S_4 symmetry axes parallel to the crystal *c* axis and differing in the identity of the bound solvent molecules (MeCN vs dioxane). There are also three dioxane and one MeOH molecules in the asymmetric unit that are disordered and could not be modeled properly. Thus program SQUEEZE,[14c] a part of the PLATON package of crystallographic software, was used to calculate the solvent disorder area and remove its contribution to the overall intensity data. A total of 646 parameters were included in the refinement using 6920 reflections with $I > 2\sigma(I)$.

For **7**·$4H_2O$·3MeCN·$2CH_2Cl_2$, the structure could not be refined to a satisfactory, publishable level because of poor diffraction and extensive ligand and solvent disorder, but we were able to confirm that it contains a Mn_8Ce core analogous to those of **4**−**6**. The asymmetric unit contains a complete Mn_8Ce cluster in a general position, and four H_2O, three MeCN, and two CH_2Cl_2 molecules. Most of the phenyl rings display considerable displacement motions but not large enough to allow resolution of different sites. Consequently, large thermal parameters are observed for their C atoms, and they were thus refined with isotropic thermal parameters. The cluster has four coordinated water molecules, as in **4**, which hydrogen bond to the four water molecules of crystallization. The latter are thus ordered, and do not bridge neighboring molecules, unlike the situation in **4**·$4H_2O$ and **4**·$4H_2O$·4MeCN. The MeCN and CH_2Cl_2 solvent molecules are severely disordered, and the program SQUEEZE was used to calculate the solvent disorder area and remove its contribution to the overall intensity data. The final R1 and wR2 were 8.91 and 21.36%, respectively. These values are similar to those for **4**·$4H_2O$, which is why we sought and obtained better crystals of what proved to be **4**·$4H_2O$·4MeCN; we were unable to obtain improved crystals of complex **7**.

Other Studies. Infrared spectra were recorded in the solid state (KBr pellets) on a Nicolet Nexus 670 FTIR spectrometer in the 400–4000 cm^{-1} range. Elemental analyses (C, H and N) were performed by the in-house facilities of the University of Florida Chemistry Department. Variable-temperature dc and ac magnetic susceptibility data were collected at the University of Florida using a Quantum Design MPMS-XL SQUID susceptometer equipped with a 7 T magnet and operating in the 1.8–300 K range. Samples were embedded in solid eicosane to prevent torquing. Magnetization vs field and temperature data were fit using the program MAGNET.[15] Pascal's constants were used to estimate the diamagnetic correction, which was subtracted from the experimental susceptibility to give the molar paramagnetic susceptibility (χ_M). Studies at ultralow temperatures (<1.8 K) were performed on single crystals at Grenoble using an array of micro-SQUIDs.[16] The high sensitivity of this magnetometer allows the study of single crystals of the order of 10−500 μm; the field can be applied in any direction by separately driving three orthogonal coils.

Results and Discussion

Syntheses. $[Mn_8CeO_8(O_2CMe)_{12}(H_2O)_4]$ (**4**) was originally obtained by accident in very small yield (5%) from an MeCN/Et_2O solution of $[Mn_6CeO_9(O_2CMe)_9(NO_3)(H_2O)_2]$[13] ($Mn^{IV}_6Ce^{IV}$) that had been left undisturbed for some time (Method B in the Experimental Section). Once the identity of **4** had been established as a Mn^{III}_8 loop with a central Ce^{IV} (vide infra) and its interesting magnetic properties identified in preliminary studies, it was considered essential to develop a rational, high-yield synthetic procedure. This was successfully developed using the linear polymer $\{[Mn(OH)(O_2CMe)_2]\cdot(MeCO_2H)\cdot(H_2O)\}_n$ (**1**) shown below.[11,17] This contains all the components found in **4**, namely Mn^{III}, carboxylate and O^{2-} (as OH^-) groups, except the Ce^{IV} ion. It was thus suspected that a reaction between the polymer

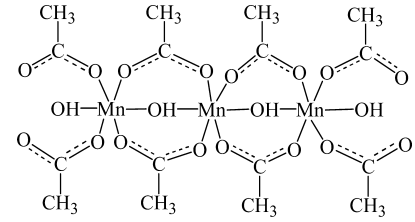

(**1**)

and a source of oxophilic Ce^{IV} with a Ce:Mn ratio of 1:8 might lead to formation of **4** as $Ce^{4+}-OH^-$ contacts develop during the reaction and the chain essentially wraps around the Ce^{IV} ion, followed by deprotonation of OH^- in the presence of carboxylate groups as H^+ acceptors. Thus, the reaction between **1** and $(NH_4)_2Ce(NO_3)_6$ in MeCN was investigated, and this did indeed give a high isolated yield of **4** (55%), as **4**·$4H_2O$·4MeCN (eq 1). The reaction is essentially thus a template procedure involving a Ce^{4+} template

$$(8/n)[Mn(OH)(O_2CMe)_2]_n + Ce^{4+} + 4H_2O \rightarrow [Mn_8CeO_8(O_2CMe)_{12}(H_2O)_4] + 4H^+ + 4MeCO_2H \quad (1)$$

around which the chain wraps. This is the overall, net process, and we make no mechanistic claims that the reaction actually involves chains in solution wrapping around the Ce^{4+} ion. In any case, polymer **1** is very insoluble in MeCN, slowly dissolving completely during the reaction, and the mechanism is likely a complicated heterogeneous one involving fragmentation of the polymer as Ce^{4+} binds.

Once the magnetic studies had established that there are weak intermolecular interactions in **4** (vide infra), derivatives of **4** were sought that (i) might have weaker intermolecular interactions as a result of replacement with other groups of

(15) Davidson, E. R. *MAGNET*; Indiana University: Bloomington, IN, 1999.

(16) Wernsdorfer, W. *Adv. Chem. Phys.* **2001**, *118*, 99.

(17) Tasiopoulos, A. J.; Wernsdorfer, W.; Abboud, K. A.; Christou, G. *Polyhedron* **2005**, *24*, 2505.

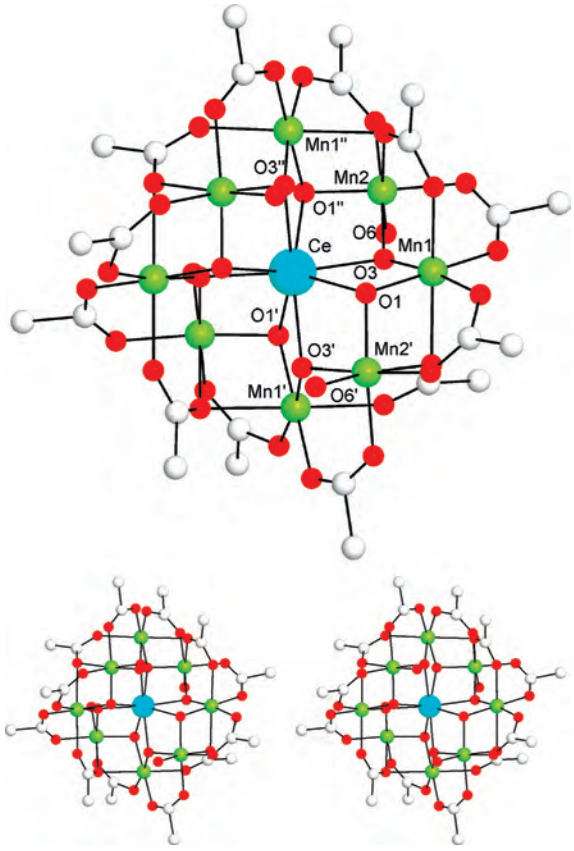

Figure 1. PovRay representation at the 50% probability level of the structure of **4** (top) and a stereoview (bottom), viewed approximately along the S_4 axis. Color scheme: Mn, green; Ce, cyan; O, red; C, grey. H atoms have been omitted for clarity.

the terminally bound water molecules, which are involved in intermolecular hydrogen-bonds, and (ii) might cause a structural perturbation that might modify the molecular properties, such as the zero-field splitting parameter, D. For point (ii), we employed bulky carboxylate groups. Since the corresponding polymer **1** was not available at the time with different carboxylates, other Mn^{III} sources were explored as routes to the desired complexes. These included $[Mn_3O(O_2CMe)_6(py)_3]$ (**2**; $2Mn^{III}$, $1Mn^{II}$) and $(NBu^n_4)[Mn_4O_2(O_2CPh)_9(H_2O)]$ (**3**; $4Mn^{III}$), which were known from previous work to be good stepping-stones to higher nuclearity complexes.[10,18,19] Indeed, the reaction of **2** with Ce^{4+} in MeCN in a 3:1 (or 8/3:1) ratio gave $[Mn_8CeO_8(O_2CMe)_{12}(py)_4]$ (**5**) in 60% isolated yield (eq 2).

$$8[Mn_3O(O_2CMe)_6(py)_3] + 3Ce^{4+} + 16H_2O \rightarrow 3[Mn_8CeO_8(O_2CMe)_{12}(py)_4] + 12py + 12MeCO_2H + 20H^+ + 8e^- \quad (2)$$

Other ratios in the 2:1 to 5:1 range gave the same product, but in lower yield. Complex **5** is the same as **4** except that the bound water groups have been replaced by pyridines. The benzoate derivative **6** was obtained from the reaction of complex **3** with $(NH_4)_2Ce(NO_3)_6$ in various ratios. Both the 2:1 and 1:1 ratios gave **6**, but the latter ratio gave the cleanest isolated product. However, **6** is $\{[Mn_8CeO_8(O_2CPh)_{12}(MeCN)_4]\ [Mn_8CeO_8(O_2CPh)_{12}(dioxane)_4]\}$, the unit cell containing two different molecules differing in the

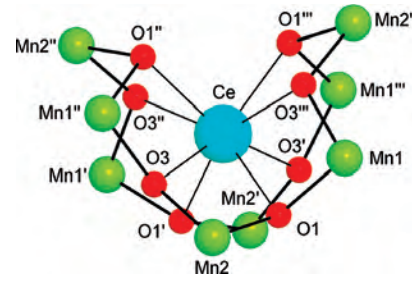

Figure 2. $[Mn_8CeO_8]$ core of **4**, which is common to complexes **4**−**7**. Color scheme: Mn, green; Ce, cyan; O, red.

bound solvent groups but, interestingly, without any disorder. The manifestation of two complexes cocrystallizing indicates the complexity of this reaction with several species likely to be in equilibrium in the reaction solution.

Finally, a derivative with very bulky diphenylacetate groups was prepared by a different procedure than those used above, because the corresponding complexes **1**−**3** with this carboxylate were not available. Instead, a carboxylate substitution reaction[3a] on complex **4** was employed; complex **4** was treated with 12–20 equiv of diphenylacetic acid in MeCN, and the reaction driven to completion by removal under vacuum of the generated acetic acid as its toluene azeotrope.[3] An excess of diphenylacetic acid also favors complete substitution, as does the higher acidity of Ph_2CHCO_2H (pK_a = 3.94) versus acetic acid (4.75). The substitution is summarized in eq 3.

$$[Mn_8CeO_8(O_2CMe)_{12}(H_2O)_4] + 12Ph_2CHCO_2H \rightarrow [Mn_8CeO_8(O_2CCHPh_2)_{12}(H_2O)_4] + 12MeCO_2H \quad (3)$$

We were pleased to see that only ligand substitution occurred during this reaction, giving the desired $[Mn_8CeO_8(O_2CCHPh_2)_{12}(H_2O)_4]$ (**7**) in 60% isolated yield, rather than cluster fragmentation.

Description of Structures. A PovRay representation and stereoview of **4** are presented in Figure 1, and a side-view of the common $[Mn_8CeO_8]$ core present in complexes **4**−**7** is shown in Figure 2 for **4**. A Povray representation of one of the molecules in complex **6** is presented in Figure 3; the structures of **5** and **7** are available in the Supporting Information. Selected metric parameters for complexes $\mathbf{4}\cdot 4H_2O$, $\mathbf{4}\cdot 4H_2O\cdot 4MeCN$, $\mathbf{5}\cdot 3C_4H_8O_2$, and $\mathbf{6}\cdot 12C_4H_8O_2\cdot 4MeOH$ are compared in Table 2.

Complex $\mathbf{4}\cdot 4H_2O$ and $\mathbf{4}\cdot 4H_2O\cdot 4MeCN$ crystallize in the tetragonal space group $I\bar{4}$ with the $[Mn_8CeO_8(O_2CMe)_{12}(H_2O)_4]$ molecule lying on a crystallographic S_4 symmetry axis. The cluster contains one Ce^{IV} and eight Mn^{III} ions bridged by eight μ_3-O^{2-} and 12 $CH_3CO_2^-$ groups (Figure 1). The structure can be described as a nonplanar, saddlelike

(18) (a) Brechin, E. K. *Chem Commun.* **2005**, 5141. (b) Piligkos, S.; Rajaraman, G.; Soler, M.; Kirchner, N.; Slageren, J.; Bircher, R.; Parsons, S.; Gudel, H.-U.; Kortus, J.; Wernsdorfer, W.; Christou, G.; Brechin, E. K. *J. Am. Chem. Soc.* **2005**, *127*, 5572. (c) Boskovic, C.; Wernsdorfer, W.; Folting, K.; Huffman, J. C.; Hendrickson, D. N.; Christou, G. *Inorg. Chem.* **2002**, *41*, 5107. (d) Brechin, E. K.; Boskovic, C.; Wernsdorfer, W.; Yoo, J.; Yamaguchi, A.; Sanudo, E. C.; Concolino, T. R.; Rheingold, A. L.; Ishimoto, H.; Hendrickson, D. N.; Christou, G. *J. Am. Chem. Soc.* **2002**, *124*, 9710.

(19) Mishra, A.; Wernsdorfer, W.; Abboud, K. A.; Christou, G. *Chem. Commun.* **2005**, 54.

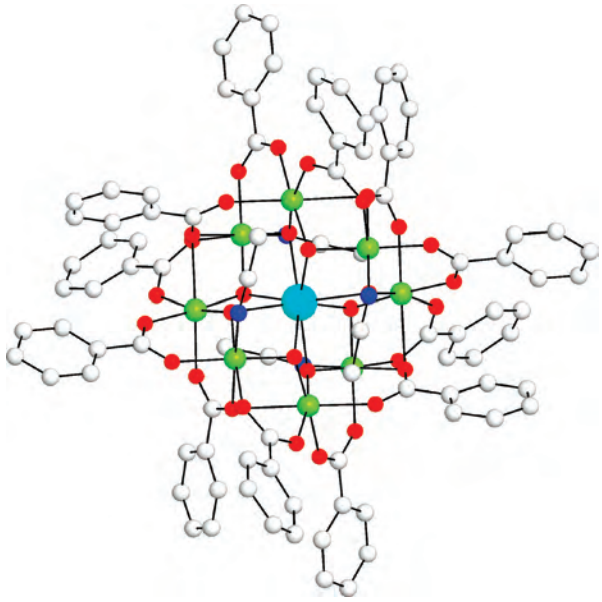

Figure 3. PovRay representation at the 50% probability level of $[Mn_8CeO_8(O_2CPh)_{12}(MeCN)_4]$, one component of the structure of **6**. Color scheme: Mn, green; Ce, cyan; N, dark blue; O, red; C, grey. H atoms have been omitted for clarity.

Table 2. Comparison of Selected Interatomic Distances (Å) and Angles (deg) for **4**–**6**

params[a]	**4**[b]	**4**[c]	**5**[d]	**6**[e,f]
Ce1···Mn1	3.345(5)	3.331(1)	3.315(1)	3.309(1)
Ce1···Mn2	3.356(5)	3.348(1)	3.330(1)	3.320(1)
Mn1···Mn2	3.240(8)	3.237(1)	3.243(1)	3.255(1)
Mn1···Mn2′	3.029(7)	3.034(1)	3.024(1)	3.011(1)
Ce1−O^{2-}	2.332(19)	2.313(3)	2.323(4)	2.307(3)
Ce1−O^{2-}	2.375(20)	2.381(3)	2.369(3)	2.390(3)
Mn1−O^{2-}	1.919(20)	1.888(3)	1.874(4)	1.867(3)
Mn1−O^{2-}	1.845(20)	1.864(3)	1.867(3)	1.856(3)
Mn2−O^{2-}	1.866(20)	1.890(3)	1.872(4)	1.878(3)
Mn2−O^{2-}	1.859(20)	1.848(3)	1.846(3)	1.844(3)
Ce1−O^{2-}−Mn1	105.8(9)	105.3(2)	104.1(2)	104.8(2)
Ce1−O^{2-}−Mn1	101.8(9)	102.0(2)	102.1(2)	101.3(2)
Ce1−O^{2-}−Mn2	105.9(9)	106.6(2)	105.4(2)	105.7(2)
Ce1−O^{2-}−Mn2	104.0(9)	102.7(2)	102.9(2)	101.5(2)
Mn1−O^{2-}−Mn2	122(1)	121.4(2)	121.7(2)	123.3(2)
Mn1−O^{2-}−Mn2′	106(1)	106.8(2)	107.7(2)	107.0(2)

[a] Atom labels as in Figures 1 and 2. [b] **4**·$4H_2O$. [c] **4**·$4H_2O$·4MeCN. [d] **5**·$3C_4H_8O_2$. [e] **6**·$12C_4H_8O_2$·4MeOH. [f] Data for the MeCN-bound molecule.

$[Mn^{III}_8(\mu_3\text{-}O)_8]^{8+}$ loop attached to a central Ce^{IV} ion via the triply bridging oxides of the loop. The resulting $[Mn_8CeO_8]^{12+}$ core is shown as a side view in Figure 2 and can be seen to comprise eight $[MnO_2Ce]$ rhombs fused at the Ce−O^{2-} edges. The four Mn2 atoms occupy the corners of an almost perfect tetrahedron (Mn2−Ce1−Mn2′ and Mn3−Ce2−Mn3′ angles in **4**·$4H_2O$ and **4**·$4H_2O$·4MeCN range from 108.35 to 111.40°), whereas the four Mn1 atoms form a distorted (flattened) tetrahedron (Mn1−Ce−Mn1′ Mn4−Ce−Mn4′ angles in **4**·$4H_2O$ and **4**·$4H_2O$·4MeCN range from 91.50 to 92.61°). Within this description, the Ce^{IV} ion occupies the center of both the Mn_4 tetrahedra. Peripheral ligation around the $[Mn_8CeO_8]^{12+}$ core is provided by eight syn, syn doubly and four triply bridging $CH_3CO_2^-$ groups. Four H_2O molecules (O6 and its symmetry counterparts) are terminal ligands on four of the Mn^{III} (Mn2 in Figure 1) ions. The Ce atom is eight-coordinate with distorted dodecahedral geometry, and the Ce−O bond lengths (2.29–2.38 Å) are typical for eight-coordinate Ce^{IV}. [20b] All the Mn atoms are six-coordinate with near-octahedral geometry and display Jahn–Teller (JT) elongation axes (vide infra), as expected for high-spin Mn^{III} ions, with the JT bonds being at least 0.1–0.2 Å longer than the other Mn^{III}−O bonds. These metal oxidation states are consistent with charge considerations within the molecule, and were confirmed by bond valence sum (BVS) calculations.[20] The obtained BVS values are shown for complexes **4**·$4H_2O$ and **4**·$4H_2O$·4MeCN in Table 3. A close examination of the packing of **4**·$4H_2O$ and of **4**·$4H_2O$·4MeCN revealed the formation of one-dimensional hydrogen-bonded chains of Mn_8Ce clusters linked by the four water molecules of crystallization, as described in the Experimental Section.

Table 3. Bond-Valence Sums for the Mn and Ce Atoms of Complex **4**·$4H_2O$·4MeCN[a]

atom	Mn^{II}	Mn^{III}	Mn^{IV}	atom	Ce^{III}	Ce^{IV}
Mn1	3.24	2.97	3.12	Ce1	4.33	3.75
Mn2	3.23	2.95	3.10			
Mn3	3.25	2.98	3.12	Ce2	4.35	3.77
Mn4	3.22	2.95	3.10			

[a] Underlined values are the ones closest to the charge for which they were calculated. The oxidation state of a particular atom can be taken as the nearest whole number to the underlined value.

Complex **5**·$3C_4H_8O_2$ crystallizes in the tetragonal space group $P4_2/n$ with the $[Mn_8CeO_8(O_2CMe)_{12}(py)_4]$ cluster again lying on a crystallographic S_4 symmetry axis (Figure S1). The molecule is essentially isostructural with complex **4**, the main difference being that the four terminal ligands are now pyridine (py) rather than H_2O as in **4**. Additionally, there are three 1,4-dioxane molecules of crystallization; as a result of these and the terminal py groups, there are now no strong hydrogen-bonding contacts between adjacent clusters. This is unlike the situation in **4** and provides for more isolated Mn_8Ce clusters in **5**. Complex **6**·$12C_4H_8O_2$·4MeOH crystallizes in the tetragonal space group $P4n2$ and contains two different Mn_8Ce clusters $[Mn_8CeO_8(O_2CPh)_{12}(MeCN)_4]$ and $[Mn_8CeO_8(O_2CPh)_{12}(C_4H_8O_2)_4]$ both lying on S_4 axes (Figure 3). The two clusters are in a 1:1 ratio and differ only in the terminal ligation by four MeCN versus four 1,4-dioxane molecules, with no disorder between them. Otherwise, each cluster is essentially isostructural with those in **4** and **5**. Complex **7**·$4H_2O$·$2CH_2Cl_2$·3MeCN crystallizes in the lower symmetry monoclinic space group $P2_1/n$ with the asymmetric unit containing the complete $[Mn_8CeO_8(O_2CCHPh_2)_{12}(H_2O)_4]$ molecule in a general position (see the Supporting Information, Figure S2). The four water molecules of crystallization form hydrogen-bonds with only one cluster, and do not provide for intermolecular linkages, unlike **4**. Other than the difference in the carboxylate group, which causes a greater separation between neighboring molecules, the cluster is again essentially isostructural with those in **4**−**6**.

Structural Comparison with $[Mn_{12}O_{12}(O_2CR)_{16}(H_2O)_4]$ Complexes. The presence of a nonplanar $[Mn_8O_8]$ loop in complexes **4**−**7** is similar to the situation within the

(20) (a) Liu, W.; Thorp, H. H. *Inorg. Chem.* **1993**, *32*, 4102. (b) Roulhac, P. L.; Palenik, G. J. *Inorg. Chem.* **2003**, *42*, 118.

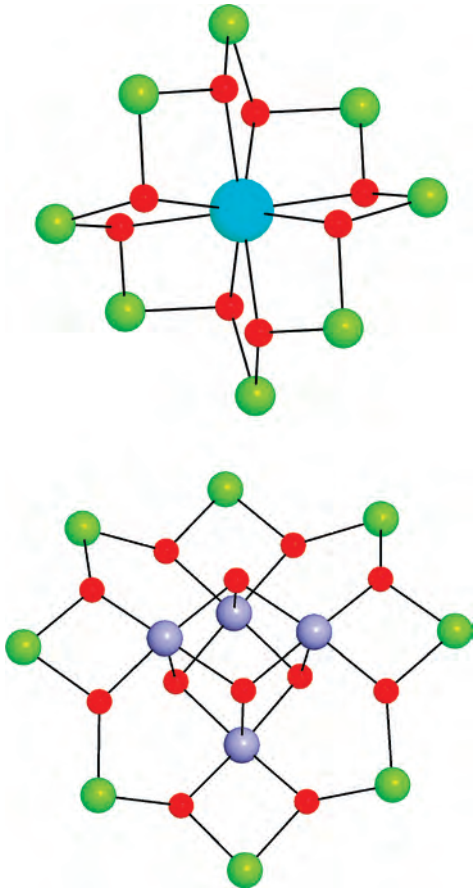

Figure 4. Comparison of the $[Mn_8CeO_8]^{12+}$ core (top) with the $[Mn_{12}O_{12}]^{16+}$ core (bottom). Color scheme: Mn^{III}, green; Mn^{IV}, violet; Ce, cyan; O, red.

$[Mn_{12}O_{12}(O_2CR)_{16}(H_2O)_4]$ (Mn_{12}) family of complexes, which are SMMs with $S = 10$ ground states.[3] These contain a nonplanar $[Mn_8O_8]$ loop that is attached via the oxide ions to the Mn^{IV} atoms of a central $[Mn_4O_4]$ cubane instead of a smaller Ce atom (Figure 4). In both cases, therefore, there are eight metal-oxide bonds between the $[Mn_8O_8]$ loop and the central unit. However, in **4**−**7**, these are all to the same atom, the central Ce^{IV}, and this rationalizes the fact that the $[Mn_8O_8]$ loop in these complexes is very far from planar, in contrast to the $[Mn_8O_8]$ loop in the Mn_{12} complexes, which is much closer to planar. The latter also precludes any of the carboxylate groups becoming triply bridging, and the Mn_{12} complexes thus have four more doubly bridging carboxylates than **4**−**7**, each bridging a loop Mn^{III} with a central Mn^{IV}.

The above structural differences between **4**–**7** and the Mn_{12} complexes lead to another difference between them, the relative alignment of their Mn^{III} Jahn–Teller (JT) elongation axes. Because the molecular anisotropy is the net tensor projection of the individual Mn^{III} anisotropies onto the molecular anisotropy axis, the relative alignments of the individual Mn^{III} JT axes, which define the single-ion anisotropy (z) axis, are crucial in controlling the magnitude of the molecular anisotropy, i.e. the molecular axial zero-field splitting parameter, D. In Mn_{12} complexes, the eight JT axes are roughly all aligned parallel to the molecular S_4 (z axis), leading to a significant net D value: for example, it is

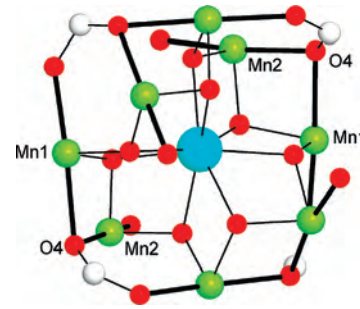

Figure 5. Common core of complexes **4**−**7** depicting the near perpendicular alignment of the Jahn–Teller (JT) pairs of axes. Thick black bonds denote JT elongation axes. Color scheme: Mn, green; Ce, cyan; O, red; C, grey.

$-0.468(2)$ cm^{-1} for $[Mn_{12}O_{12}(O_2CCH_2Br)_{16}(H_2O)_4]\cdot 4CH_2Cl_2$.[21] In contrast, the JT axes in **4**−**7** have no preferred orientation. The JT axes are shown in Figure 5 as solid black bonds, and they can be seen to be disposed essentially equally with respect to any chosen reference direction. This is facilitated by the fact that they occur in four symmetry-related pairs of JT axes that intersect at the same O atom and thus are nearly perpendicular, with the Mn2−O4−Mn1 angle being 83.9°. Indeed, for all the complexes **4**−**7**, the eight JT axes occur in sets of two with the Mn−O−Mn intersection angle being in the range of 80–84°. This and the actual or virtual S_4 symmetry are expected to lead to a very low anisotropy (small $|D|$ value), and this was borne out by the experiment (vide infra).[9]

DC Magnetic Susceptibility Studies for Complexes 4, 5, and 7. Solid-state variable temperature magnetic susceptibility measurements were performed on vacuum-dried microcrystalline samples of representative complexes **4**·$4H_2O$, **5**·$3C_4H_2O_2$, and **7**·$4H_2O$ suspended in eicosane to prevent torquing. The dc magnetic susceptibility (χ_M) data were collected in the 5.0–300 K range in a 0.1 T magnetic field and are plotted as $\chi_M T$ vs T in Figure 6. For **4**, the $\chi_M T$ value of 39.36 cm^3 K mol^{-1} at 300 K remains essentially constant down to 70 K and then steadily increases with decreasing temperature to 69.28 cm^3 K mol^{-1} at 5.0 K indicating predominantly ferromagnetic coupling in **4** and a large ground-state spin S. For **5**, the $\chi_M T$ value of 28.31 cm^3 K mol^{-1} at 300 K also remains essentially constant to 70 K and then steadily decreases with decreasing temperature to 17.08 cm^3 K mol^{-1} at 5.0 K indicating a relatively small ground state S for **5**. For **7**, the $\chi_M T$ of 28.00 cm^3 K mol^{-1} at 300 K is essentially constant down to ~120 K and then increases to a maximum of 32.47 cm^3 K mol^{-1} at 70 K, and then decreases to 19.85 cm^3 K mol^{-1} at 5.0 K, again indicating a relatively small ground S for **7**. The spin-only ($g = 2.0$) value for eight noninteracting, high-spin Mn^{III} ions is 24.00 cm^3 K mol^{-1} (Ce^{IV} is diamagnetic, f^0). For each compound, the high-temperature $\chi_M T$ values are above this, most notably for **4**. This suggests that the dominant exchange interaction within the molecules is ferromagnetic, and then

(21) (a) Chakov, N. E.; Lawrence, J.; Harter, A. G.; Hill, S. O.; Dalal, N. S.; Wernsdorfer, W.; Abboud, K. A.; Christou, G. *J. Am. Chem. Soc.* **2006**, *128*, 6975. (b) Tsai, H.-L.; Chen, D.-M.; Yang, C.-I.; Jwo, T.-Y.; Wur, C.-S.; Lee, G.-H.; Wang, Y. *Inorg. Chem. Commun.* **2001**, *4*, 511. (c) An, J.; Chen, Z.-D.; Zhang, X.-X.; Raubenheimer, H. G.; Esterhuysen, C.; Gao, S.; Xu, G.-X. *Dalton Trans.* **2001**, *22*, 3352.

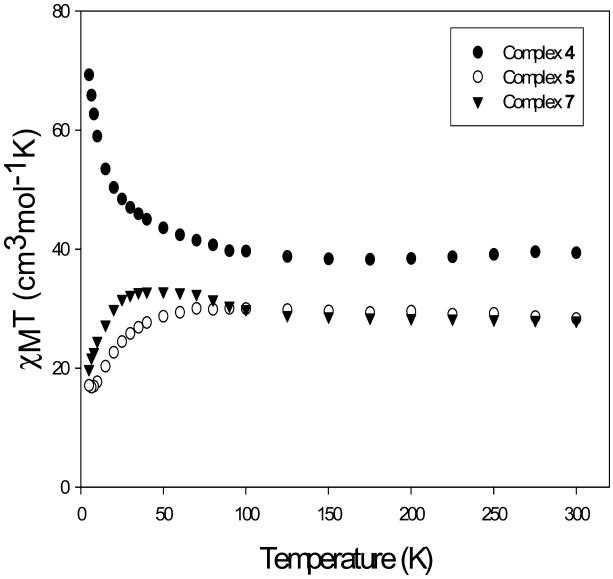

Figure 6. Plots of dc $\chi_M T$ vs T for complexes **4**, **5**, and **7**.

weaker interactions (antiferro- and/or ferromagnetic) assume greater importance at lower temperatures (vide infra).

The eight Mn^{III} centers in **4**, **5**, and **7** will give total S values in the range 0 to 16. Owing to the size and low symmetry of the molecules, a matrix diagonalization method to evaluate the various Mn_2 pairwise exchange parameters (J_{ij}) within the Mn_8Ce cores is not easy. Similarly, application of the equivalent operator approach based on the Kambe vector coupling method is not possible.[22] Therefore, we focused only on identifying the ground state S values for the complexes since these would in any case dominate the low temperature studies we performed. Hence, magnetization (M) data were collected in the 0.1–7 T magnetic field and 1.8–10 K temperature ranges. The data were fit, using the program MAGNET,[15] by diagonalization of the spin Hamiltonian matrix assuming only the ground-state is populated, incorporating axial anisotropy ($D\hat{S}_z^2$) and Zeeman terms, and employing a full powder average. The corresponding spin Hamiltonian (H) is given by eq 4,

$$H = D\hat{S}_z^{\,2} + g\mu_B\mu_0\hat{S}H \qquad (4)$$

where D is the axial anisotropy (ZFS) constant, μ_B is the Bohr magneton, $\hat{S}_z$ is the easy-axis spin operator, g is the electronic g factor, μ_0 is the vacuum permeability, and H is the applied field. The last term in eq 4 is the Zeeman energy associated with an applied magnetic field. The data for **4** are plotted as reduced magnetization ($M/N\mu_B$) versus H/T in Figure 7, and the fit (solid lines) gave $S = 16$, $D = -0.10$ cm^{-1}, and $g = 1.98$. When data collected at fields <3.0 T were included, a satisfactory fit could not be obtained, which is as expected from the crystal structure described above, which revealed intermolecular hydrogen-bond linkages between Mn_8Ce clusters that will introduce intermolecular exchange interactions that are not included in the fitting model; the use of only higher field data overcomes the intermolecular exchange interactions and their effect on the

(22) Kambe, K. *J. Phys. Soc. Jpn.* **1950**, *48*, 15.

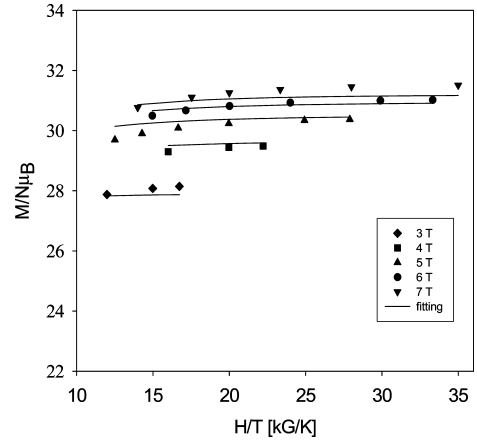

Figure 7. Magnetization (M) vs field (H) and temperature (T) data, plotted as reduced magnetization ($M/N\mu_B$) vs H/T for complex **4** at applied fields of 3−7 T and in the 1.8–10 K temperature range. The solid lines are the fit of the data; see the text for the fit parameters.

observed magnetization. The small D value of only -0.1 cm^{-1} is consistent with the complex having the JT axes almost perpendicular, as stated earlier, and the $g < 2$ value is as expected for Mn.

For complexes **5**·$3C_4H_8O_2$ and **7**·$4H_2O$, which from Figure 6 clearly have smaller spin ground states than **4**·$4H_2O$, we could not get satisfactory fits using all the data. For **5**, a somewhat reasonable fit was obtained when only data collected in the 0.1–2 T applied field range were used, and this gave $S = 5$, $D \approx -0.30$ cm^{-1} and $g \approx 1.83$ (see the Supporting Information). For **7**, a slightly better fit was obtained with data collected in the 0.1–0.8 T range, and this gave $S = 6$, $D \approx -0.34$ cm^{-1} and $g \approx 1.89$. Although the values of D and g carry significant estimated uncertainty (±20%), the ground state S values are considered reliable to ± 1 units, and are consistent with the estimates from the dc magnetic susceptibility plots in Figure 6. Such problems in fitting dc magnetization data are commonly encountered when there are low-lying excited-states (relative to kT), some of which have S values greater than that of the ground state; this is typical of systems that contain weakly antiferromagnetic interactions and/or are high nuclearity and there is thus a high density of spin states. Thus, low-lying excited states are populated, even at these relatively low temperatures, and/or the M_S levels from nearby excited states with S greater than that of the ground-state are sufficiently stabilized by the applied dc field that they thus approach or even cross the ground-state levels. Since the fitting routine assumes population of only the ground state, these excited states complicate the fitting. This is undoubtedly the problem with complexes **5** and **7**, and this is supported by the slope observed in the in-phase ac susceptibility vs temperature data (vide infra). As will be described below, ac susceptibility studies, which avoid the complications from a dc field, support the conclusions from the magnetization fits of the ground state S values for **5** and **7**.

AC Magnetic Susceptibility Studies. The values of $S = 16$ and $D = -0.10$ cm^{-1} obtained for **4**·$4H_2O$ suggested an upper limit to its barrier U to magnetization relaxation (reorientation) of $U = S^2|D| = 25.6$ cm^{-1}. Even though the

true, or effective barrier U_{eff}, would be significantly smaller due to quantum tunneling of the magnetization (QTM) through the barrier, it still suggested that at least **4**·$4H_2O$, and perhaps even **5** and **7**, might display slow relaxation at low enough temperatures, and this was explored using ac susceptibility measurements.

Alternating current magnetic susceptibility studies were performed on vacuum-dried microcrystalline samples of **4**·$4H_2O$, **5**·$3C_4H_8O_2$, and **7**·$4H_2O$ in a zero dc field in the temperature range 1.8–10 K, using a 3.5 G ac field oscillating at frequencies between 5 and 1000 Hz. If the magnetization vector can relax fast enough to keep up with the oscillating field, then there is no imaginary (out-of-phase) susceptibility signal (χ_M''), and the real (in-phase) susceptibility (χ_M') is equal to the dc susceptibility. [23] However, if the barrier to magnetization relaxation is significant compared to thermal energy (kT), then there is a nonzero χ_M'' signal and the in-phase signal decreases. In addition, the χ_M'' signal will be frequency-dependent. For complexes **4**−**7**, there were no significant out-of-phase χ_M'' signals observed down to 1.8 K, the operating minimum of our SQUID magnetometer; only the very beginnings of a χ_M'' signal was observed for each compound to this temperature, the most evident being for **4**. This suggested that temperatures much lower than 1.8 K would have to be employed to better gauge whether **4**−**7** might be single-molecule magnets (SMMs).

Since the in-phase susceptibility (χ_M') is equal to the dc susceptibility (χ_M) when there is no χ_M'' component, the χ_M' signal is a useful way of determining (or confirming) the ground state S of a species in the presence of low-lying excited states because it precludes the potential complications that arise from a dc field. In such cases, obtaining the ground state S from ac data is invaluable.[24] The ac χ_M' is shown as $\chi_M'T$ vs T for **4**, **5**, and **7** in Figure 8. The χ_M'T value for **4** is 63.17 cm^3 mol^{-1} K at 10 K and increases steeply with decreasing temperature to 94.05 cm^3 mol^{-1} K at 1.8 K, where it begins to taper off concomitant with the beginnings of a χ_M'' signal and weak intermolecular interactions (vide infra). Extrapolating the steep rise to 0 K, where only the ground state will be populated, using data from >2.4 K (to avoid the low T tapering) gives a $\chi_M'T$ of ∼125 cm^3 mol^{-1} K, which indicates an $S = 16$ round state with $g \approx 1.92$ (from the formula $\chi_M'T = (g^2/8)S(S+1)$), in satisfying agreement with the magnetization fit. Such a high $\chi_M'T$ is also consistent with $S = 15$ but with g ≈ 2.04, which is not expected for Mn; in any case, it is not clear how an $S = 15$ ground-state could arise for a molecule with S_4 symmetry (vide infra). The ac $\chi_M'T$ vs T data thus support the conclusion from the magnetization fit of an $S = 16$ ground state for **4**. The decrease in $\chi_M'T$ with increasing temperature is due to thermal population of excited states with $S < 16$, as expected since $S = 16$ is the maximum possible for a Mn^{III}_8 complex. However, the particularly steep decrease attests to only very small energy gaps to the excited states, i.e., they are very low-lying and rapidly become populated even with only small temperature increases.

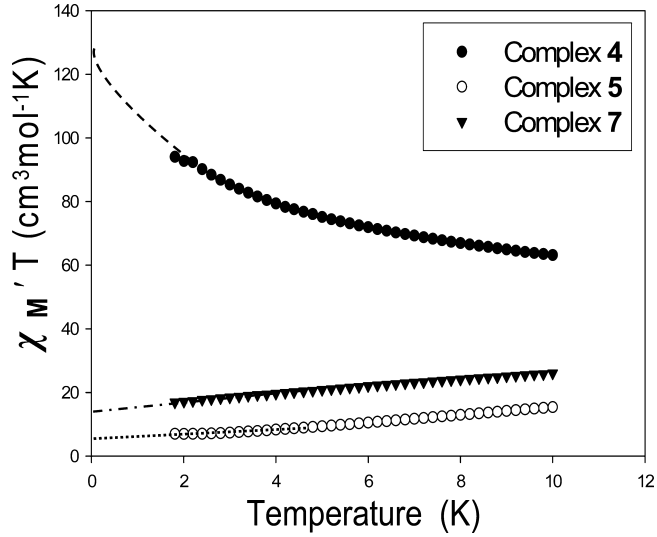

Figure 8. Plots of ac $\chi_M'T$ vs T for complexes **4**, **5**, and **7** at a 500 Hz ac frequency.

The $\chi_M'T$ vs T plots for **5** and **7** in Figure 8 are similar to each other and very different to that for **4**, as was also seen in the dc χ_MT vs T plots of Figure 6. The plots show a steady decrease with decreasing temperature, and $\chi_M'T$ reaches 6.98 and 16.88 cm^3 mol^{-1} K at 1.8 K for **5** and **7**, respectively. Linear extrapolation to 0 K gives values of ∼6.7 and ∼16 cm^3 mol^{-1} K for **5** and **7**, respectively. The latter suggests an $S = 6 \pm 1$ ground state for **7**, with $g < 2$ as expected for Mn; the spin-only ($g = 2.0$) values for $S = 5$, 6, or 7 states are 15, 21, and 28 cm^3 mol^{-1} K. The value for **5** of ∼6.7 cm^3 mol^{-1} K is suggestive of an $S = 4$ or 5 ground state; the spin-only ($g = 2.0$) values for $S = 3$, 4, or 5 states are 6, 10, and 21 cm^3 mol^{-1} K. For both compounds, the $\chi_M'T$ increases with increasing temperature indicating population of low-lying excited states with S greater than that of the ground state, and rationalizes the problems in fitting the DC magnetization data, which assumes population of only a single state.

Because complex **4** displays the beginnings of frequency-dependent out-of-phase χ_M' signals, which are an indication of the superparamagnet-like slow magnetization relaxation of a SMM, we decided to investigate this further. Out-of-phase χ_M'' signals are a necessary but not sufficient proof of an SMM,[25] and thus we collected dc magnetization data to lower temperature (<1.8 K).

Hysteresis Studies below 1.8 K. The observation of hysteresis loops in magnetization vs applied dc field studies represents the diagnostic property of a magnet, including SMMs and superparamagnets below their blocking temperature (T_B). Thus, such data were collected down to 0.04 K on single crystals of **4**·$4H_2O$, **5**·$3C_4H_8O_2$ and **7**·$4H_2O$·

(23) Novak, M. A.; Sessoli, R. In *Quantum Tunnelling of Magnetization*, QTM'94; Gunther, L.; Barbar, B., Eds.; Kluwer: Dordrecht, The Netherlands, 1995; pp 171–188.

(24) (a) King, P.; Wernsdorfer, W.; Abboud, K. A.; Christou, G. *Inorg. Chem.* **2005**, *44*, 8659. (b) Soler, M.; Wernsdorfer, W.; Folting, K.; Pink, M.; Christou, G. *J. Am. Chem. Soc.* **2004**, *126*, 2156. (c) Sañudo, E. C.; Wernsdorfer, W.; Abboud, K. A.; Christou, G. *Inorg. Chem.* **2004**, *43*, 4137.

(25) (a) Chakov, N. E.; Wernsdorfer, W.; Abboud, K. A.; Christou, G. *Inorg. Chem.* **2004**, *43*, 5919. (b) Mishra, A.; Tasiopoulos, A. J.; Wernsdorfer, W.; Abboud, K. A.; Christou, G. *Inorg. Chem.* **2007**, *46*, 3105. (c) Boskovic, C.; Pink, M.; Huffman, J. C.; Hendrickson, D. N.; Christou, G. *J. Am. Chem. Soc.* **2001**, *123*, 9914.

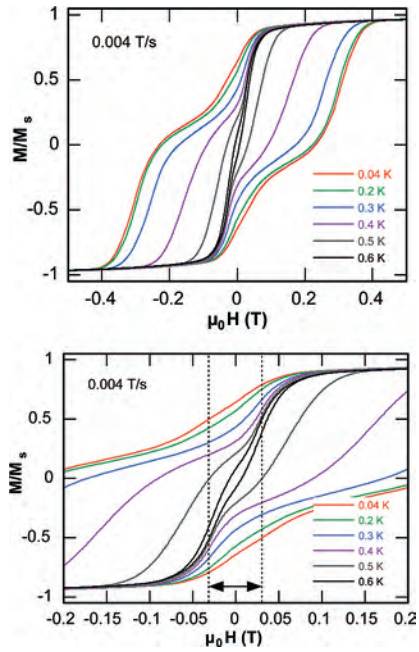

Figure 9. (top) Magnetization (M) vs applied magnetic field (H) hysteresis loops for a single crystal of **4**·$4H_2O$ at a 0.004 T/s sweep rate in the 0.04–0.6 K temperature range; and (bottom) expansion of the 0.2 to –0.2 T field range showing the exchange-bias measurement positions. M is normalized to its saturation value, M_S.

$3MeCN\cdot 2CH_2Cl_2$ (stored in mother liquor) using a micro-SQUID apparatus.[16] The observed magnetization responses for complex **4** are shown in Figure 9 at a sweep rate of 0.004 T/s and at different temperatures. Hysteresis loops are clearly evident below 0.6 K, with the coercivity (half the loop width at $M/M_S = 0$) increasing with decreasing temperature, as expected for the superparamagnet-like properties of a SMM. A dominating feature in the loops is the two-step profile of the QTM and the fact that on sweeping the field back from either extreme toward zero field, the magnetization begins to decrease before reaching zero field. This shift from zero field is indicative of an exchange bias[26] from neighboring molecules, i.e., the influence of intermolecular antiferromagnetic exchange interactions on the magnetization relaxation dynamics of a molecule. This is totally consistent with the observation in the crystal structure of **4**·$4H_2O$ of one-dimensional chains of Mn_8Ce molecules linked by hydrogen-bonded bridging solvate water molecules (see Figure S5 of the Supporting Information), and there are likely also some contributions from intermolecular dipolar interactions between the large ground state $S = 16$ spins. Similar behavior has been seen in the Fe_{19} SMMs,[27] which also exhibit intermolecular interactions. As reported elsewhere, both for isolated dimers of interacting molecules[26] and also three-dimensional networks of interacting molecules,[28] the strength of the intermolecular exchange coupling constant J can be calculated from the field shift that it causes in the hysteresis

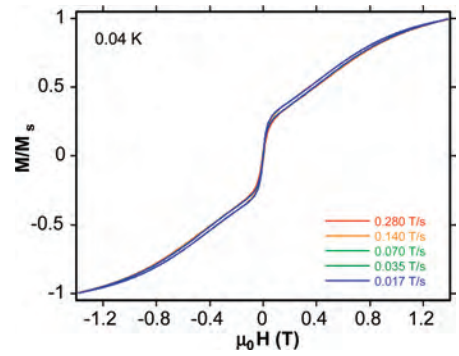

Figure 10. Magnetization (M) vs applied magnetic field (H) hysteresis loops for a single crystal of **5**·$3C_4H_8O_2$ at 0.04 K for the indicated field sweep rates. M is normalized to its saturation value, M_S.

loops. Closer inspection of the hysteresis loop (Figure 9, bottom) indicates an exchange-bias of 30 mT either side of zero field. From this can be calculated J by using the expression in eq 5, appropriate for the $H = -2J\hat{S}_i\cdot\hat{S}_j$ convention,

$$J = -g\mu_B\mu_o H_{ex}/k_B S \qquad (5)$$

where H_{ex} is the exchange-bias field (i.e., the shift from zero field), k_B is the Boltzmann constant, and the other symbols are as defined for eq 4. [28] This gives $J = -0.0012$ K, and from this can be calculated the exchange interaction energy $-2JS^2$ of 0.65 K. The interaction is thus antiferromagnetic, as expected, and very weak. Complex **4** is thus a SMM that also exhibits weak antiferromagnetic interactions along a one-dimensional hydrogen-bonded chain. Note that the latter half of this statement does not contradict the former: no assembly of SMM molecules in a crystal can ever be completely free of all possible interactions with neighbors (otherwise it would be a gas), and the important question is then exactly how strong are these interactions from a magnetic point of view. If they are weak, as they are for **4**, then they are merely a perturbation of the single-molecule magnetic properties, and a compound such as **4** can be described as an exchange-biased SMM.[26] If intermolecular interactions are relatively strong, however, then the crystal is best described as containing antiferromagnetically ordered 1-, 2- or 3D extended networks.

The magnetization vs field responses for complex **5**·$3C_4H_8O_2$ at 0.04 K and different scan rates are shown in Figure 10. There is essentially no hysteresis observed even at the highest scan rates, and there is also a strongly sloping background as the field is increased from zero. These observations confirm that **5** is not a SMM, and that there are very low lying excited states with S greater than that of the ground state whose levels cross with those of the latter leading to increased values of the magnetization at increasing fields. These data support the conclusions from the ac in-phase data.

The magnetization vs field responses for complex **7**·$4H_2O\cdot 3MeCN\cdot 2CH_2Cl_2$ are plotted in Figure 11, showing both the temperature dependence at 0.14 T/s and the scan-rate dependence at 0.04 K. Hysteresis is observed whose coercivity increases with decreasing temperature and increasing scan rate, as expected for a superparamagnetlike SMM. In

(26) (a) Wernsdorfer, W.; Aliaga-Alcalde, N.; Hendrickson, D. N.; Christou, G. *Nature,* **2002**, *416*, 406. (b) Hill, S.; Edwards, R. S.; Aliaga-Alcalde, N.; Christou, G. *Science* **2003**, *302*, 1015.
(27) Goodwin, J. C.; Sessoli, R.; Gatteschi, D.; Wernsdorfer, W.; Powell, A. K.; Heath, S. L. *J. Chem. Soc., Dalton Trans.* **2000**, 1835.
(28) Tiron, R.; Wernsdorfer, W.; Aliaga-Alcalde, N.; Christou, G. *Phys. Rev. B* **2003**, *68*, 140407(1–4)

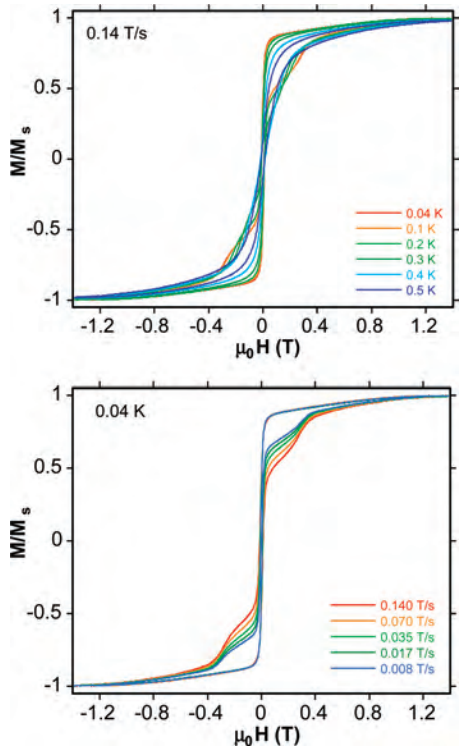

Figure 11. Magnetization (M) vs applied magnetic field (H) hysteresis loops for a single crystal of **7**·4H_2O·3MeCN·2CH_2Cl_2: (top) in the temperature range 0.04–0.5 K at a 0.14 T/s sweep rate; (bottom) in the 0.008–0.140 T/s sweep rate range at 0.04 K. M is normalized to its saturation value, M_S.

contrast to the behavior of **4**, the magnetization does not begin to relax until zero field is reached. This shows that there is no noticeable exchange-bias and thus no significant intermolecular interactions, as expected from the crystal structure, which shows noninteracting molecules. The clearly dominating feature in the loops is the large step at zero field due to quantum tunneling of the magnetization (QTM). The large size of this step corresponds to most (75–80%) of the magnetization reversing, and thus the only other observed step at ~0.3 T is very small by comparison. The large size of the step reflects a fast QTM rate, which is consistent with the low site-symmetry of this molecule; unlike complexes **4**−**6**, **7** does not have S_4 (axial) symmetry but only crystallographic C_1 (rhombic) symmetry. This leads to a significant transverse term in the spin Hamiltonian, which greatly mixes levels on either side of the anisotropy barrier and leads to correspondingly increased tunneling rates.[29] Unfortunately, this fast relaxation at zero field precludes collection of magnetization vs time decay data with which to construct an Arrhenius plot in order to determine the effective barrier to relaxation (U_{eff}). However, the field separation between steps (ΔH) of 0.3 T in Figure 11 allows the lower limit of the $|D|/g$ value of **7** to be obtained from the expression

$$|D|/g = \mu_B \Delta H \qquad (6)$$

in eq 6, and this gives $|D|/g = 0.14$ cm^{-1}. Assuming $g = 2$ and $D < 0$, this then gives $D = -0.28$ cm^{-1}, which is in reasonable agreement with the $D \approx -0.34$ cm^{-1} obtained from the magnetization fit. Note that, as stated, eq 6 gives the lower limit to D because of the strong mixing of levels due to the low symmetry; this causes the large step at zero field, but there will be even stronger mixing at the first nonzero step and the magnetization therefore relaxes completely before the field reaches the value of the first nonzero field step. It thus makes sense that the obtained value of $D = -0.28$ cm^{-1} is less than the $D \approx -0.34$ cm^{-1} from the magnetization fit.

Rationalization of the Variable Spin in Mn_8Ce Complexes. One of the results of this work that warrants specific comment is the ability of the Mn_8Ce complexes to possess different ground state S values. Inspection of Figure 1 shows that the Mn_8Ce core with S_4 symmetry contains only two types of near-neighbor J_{ij} exchange constants, J_{12} and $J_{12'}$ (and their symmetry partners). If next-nearest-neighbor interactions are assumed to be zero or negligible, there are only two possibilities: (i) if J_{12} and $J_{12'}$ are both ferromagnetic, they will give an $S = 16$ ground state, as seen for **4**; and (ii) if they are both antiferromagnetic, or one is antiferromagnetic and the other is ferromagnetic, they will give an $S = 0$ ground state. Therefore, the only way to rationalize the intermediate spin values found for **5** and **7** is to accept that next-nearest-neighbor interactions are not, in fact, negligible relative to J_{12} and $J_{12'}$. No doubt this is facilitated by the Ce^{IV} ion providing additional pathways for next-nearest-neighbor interactions than would be available in an M_x wheel with nothing in the center. There are four symmetry-independent next-nearest-neighbor interactions, and the magnetic properties of the Mn_8Ce complexes are thus determined by a total of six interactions, some of which will be competing. The two types of nearest-neighbor Mn_2 interactions are both propagated via [$Mn_2(\mu$-$O^{2-})(\mu$-$O_2CR^-)_2$] bridges, but differ in that one case (e.g., Mn1−Mn2′ for **4** in Figure 1) there is one monoatomically bridging carboxylate in addition to the monoatomically bridging O^{2-}, whereas in the other case only the O^{2-} is monoatomically bridging. As a result: (i) the Mn···Mn separations in the former case (~3.0 Å) are slightly shorter than in the latter (~3.2 Å); and (ii) the angles at monoatomically bridging ligands in the former (for **4**, Mn1−O1−Mn2′ = 106.33° and Mn1−O4−Mn2′ = 83.93°, average 95.13°) are much more acute than in the latter (Mn1−O3−Mn2 = 121.98°). Two monoatomic bridges between a pair of metal atoms, and the resulting acute bridging angles they foster, can often give ferromagnetic coupling for many metals including dinuclear Mn^{III} complexes.[30] The other symmetry type of Mn_2 pair has a single monatomic μ-O^{2-} bridge as well as two carboxylate bridges, and such units in dinuclear Mn^{III} chemistry are known to typically have Mn−O−Mn angles of 123 ± 5° and to give weakly ferro- or antiferromagnetic interactions in the $-5 < J < +10$ cm^{-1} range.

On the basis of the above observations, our rationalization for the ground states seen for the Mn_8Ce complexes is as

(29) Aliaga-Alcalde, N.; Edwards, R. S.; Hill, S. O.; Wernsdorfer, W.; Folting, K.; Christou, G. *J. Am. Chem. Soc.* **2004**, *126*, 12503.

(30) (a) Beghidja, C.; Rogez, G.; Kortus, J.; Wesolek, M.; Welter, R. *J. Am. Chem. Soc.* **2006**, *128*, 3140. (b) Clerac, R.; Miyasaka, H.; Yamashita, M.; Coulon, C. *J. Am. Chem. Soc.* **2002**, *124*, 12837.

follows: the coupling within both types of nearest-neighbor Mn_2 pairs is weakly ferromagnetic in complex **4**, and sufficiently stronger than the (presumably) antiferromagnetic next-nearest-neighbor interactions to give the observed $S = 16$ ground state, but with very low-lying excited states. In **5** and **7**, however, one or both of the nearest-neighbor interactions is antiferromagnetic and comparable with next-nearest-neighbor interactions; as a result, there are competing interactions of comparable magnitude within the core, and thus spin frustration effects give a ground-state that is intermediate between the maximum ($S = 16$) and minimum ($S = 0$) possible. The exact ground-state is acutely sensitive in such situations to the relative magnitudes of the competing interactions, and thus small structural differences between **5** and **7** lead to different ground states for the two complexes. In both cases, there will again be low-lying excited states. Alternatively, one could argue that perhaps the nearest-neighbor interactions are ferromagnetic in all cases and what is varying is the strength of antiferromagnetic next-nearest-neighbor interactions. This is certainly also a possibility, but we see no reason why the next-nearest-neighbor interactions should be relatively more sensitive to small structural changes than the nearest-neighbor ones. In any event, the safest conclusion to be drawn is that the precise ground states in this family of Mn_8Ce complexes are determined by the relative magnitudes of several weak-to-very-weak exchange interactions either side of zero, and thus are acutely sensitive to what in an absolute sense are small changes of perhaps only 1 or 2 cm^{-1} in either direction.

The logical next step is to try to identify which structural change(s) is (are) primarily responsible for the change in the magnetic properties, with the likeliest candidates being the Mn−O−Mn angles. The comparative listings in Table 2 are therefore of some interest. However, within the estimated standard deviations in the crystallographic structural parameters, and the poor quality of the structure of **7**, it is not possible to identify one or more real and statistically significant structural differences between the complexes. In any case, on the basis of the above discussion, the changes in the exchange interactions required to cause the observed change in magnetic properties will be small, and thus can be caused by small structural perturbations difficult to identify above experimental uncertainties.

Conclusions

We have shown that convenient, high-yield methods are available that allow access into a new family of Mn_8Ce complexes that are new additions to the area of single-molecule magnetism. The prototype of this family was complex **4**, an SMM with $S = 16$, which displays hysteresis in magnetization vs dc field sweeps, albeit with the characteristic signature of exchange-bias, i.e. a perturbation to its single-molecule properties from the hydrogen bonding that forms 1D chains in the crystal. In an attempt to remove these intermolecular interactions, we have developed methods to derivatives of **4** in which the terminal water molecules have been replaced by pyridines, or in which the acetate groups have been replaced with other, bulkier carboxylates. These have indeed successfully provided other Mn_8Ce complexes that are SMMs. However, these changes have also had an unforeseen consequence in that they have altered the magnitude of the intramolecular exchange interactions sufficiently to lead to major changes in the ground state S values of the complexes, from the $S = 16$ for **4**, to $S = 4$ or 5 for **5**, and $S = 6 \pm 1$ for **7**. This prevents a detailed study of the hysteresis response and other properties of these complexes as a function of the molecular separations, our original objective. Nevertheless, the work did provide a second SMM, complex **7**, with no exchange-bias and with faster QTM rates as a consequence of its lower site-symmetry. From an alternative viewpoint, it is of course interesting and unusual for a given structural type to be capable of adopting such different spin ground states, and in some ways is another example of the "spin tweaking" phenomenon, as recently reported for a Mn_{25} SMM, which can be prepared as $S = {}^{51}/_{2}$ or $S = {}^{61}/_{2}$, depending on the peripheral ligands.[31]

Finally, we note that the use of a highly charged Ce^{IV} ion has led to significantly different structural chemistry than would be found with just Mn^{III} and carboxylate groups alone, and we are investigating further the new chemistry that remains to be discovered with this combination, which is also complementary to the related Mn^{IV}/Ce^{IV} and $Mn^{III}/Ce^{III}/Ce^{IV}$ chemistry we have recently reported.[13,25b]

Acknowledgment. We thank the National Science Foundation (CHE-0414555) for support of this work.

Supporting Information Available: X-ray crystallographic data in CIF format for complexes **4**·$4H_2O$, **4**·$4H_2O$·4MeCN, **5**·$3C_4H_2O_2$, **6**·$12C_4H_8O_2$·4MeOH, and **7**·$4H_2O$·3MeCN·$2CH_2Cl_2$; PovRay representations of **5** and **7**, and the reduced magnetization fits for **5** and **7** (PDF). This material is available free of charge via the Internet at http://pubs.acs.org.

IC8001064

(31) (a) Murugesu, M.; Habrych, M.; Wernsdorfer, W.; Abboud, K. A.; Christou, G. *J. Am. Chem. Soc.* **2004**, *126*, 4766. (b) Stamatatos, T. C.; Abboud, K. A.; Wernsdorfer, W.; Christou, G. *Angew. Chem., Int. Ed.* **2007**, *46*, 884.